Performances of an RSSI-based positioning and tracking algorithm

Ada Vittoria Bosisio
CNR/IEIIT c/o Politecnico di Milano, Milano, Italy. Email: bosisio@elet.polimi.it

***Abstract*—This paper reports the results of a positioning and tracking algorithm for indoor environments based on simulated and pre-computed attenuation map values. The localization is performed through a global optimization that minimizes a cost function computed in the data-space, which is the attenuation reference map relative to the environment under test. The tracking is implemented introducing a correlation between the current position and the previous ones. Two environments of different size, shape and characteristics are chosen for the algorithm validation.**

***Keywords*—WSN Localization; Dense Multipath; Global optimization.**

I. INTRODUCTION

The estimate of the RSSI (Received Signal Strength Intensity) is a straightforward technique to locate an object in an indoor environment when using as infrastructure a network composed of wireless sensor nodes.

As well known, such a strategy is based upon the inverse relationship between the signal attenuation and the distance receiver-transmitter. In an homogeneous environment the position of the blind node could be retrieved by means of trilateration, provided an optimal transmitting nodes deployment [1]. Unfortunately, this is not true in actual indoor environments characterized by dense multipath originated by signal interactions with walls, roof and ceiling, people moving around and/or different position of furniture and objects. The almost continuously changing scenario results in signal fluctuations that contribute to both path loss (*large scale* behavior) and local field variations *(small scale* behavior).

The proposed technique is based on pre-computed attenuation maps of the received signal inside the environment under test (EUT). The attenuation values are obtained through 2D ray tracing modeling and they are validated against measurements.

The power mapping based on a pure deterministic description does not include any signal fluctuations due to dense multipath effects. On the other side, a pure statistical characterization of the multipath channel could neglect specific environment-related behaviors [2]. Hence, a numerical modeling is adopted to produce perturbed attenuation maps of the received power. These latter ones are obtained by randomly placing in the geometrical model of the environment a varying number of scatterers of different size and electromagnetic properties.

The perturbed attenuation maps thus computed are used to represent the power fluctuations that the signal experiences in actual conditions.

The predicted values are validated through a calibration procedure against measurements. A reference map that describes the expected received power is obtained from the average of the perturbed maps. The perturbed maps are used to locate the probe node (unknown location) through the exhaustive exploration of the candidate position in the data space, i.e. the reference map for the environment under test.

The positioning algorithm works as follows: a probe node is placed in the environment under test at a given location (x_i,y_i) and one perturbed attenuation map out of the whole database assigns the attenuation values to that location. The probe node is located by minimizing a cost function K, expressed as the Euclidean distance between the attenuation values in the actual location and those in all the points of the reference attenuation map.

The tracking (non static localization) is performed through the addition of some correlation between the current probe node position with previous locations.

A. Experimental setup

The proposed algorithm was validated in two indoor environments with different characteristics: a conference room (EUT1) and a laboratory with four rooms (EUT2), whose geometry, together with the deployed wireless sensor networks (WSNs), is sketched in Figs. 1 and 2 respectively.

In the EUT1 case, the attention is focused on the ray tracing capabilities of reproducing the field behavior in a single well-controlled environment with reflections and reverberations. In the second case, EUT2, the aim is to prove if an unique cost function is capable to locate points positioned in different rooms without any information about the best server, i.e. the closer transmitting antenna. EUT1 is equipped with 8 transmitting nodes (APs) and 27 calibration points [3], while EUT2 has a network of 6 APs and 92 calibration points [4,5]. In both cases, the WSN is composed of Crossbow MICA2 devices operating at 433 MHz.

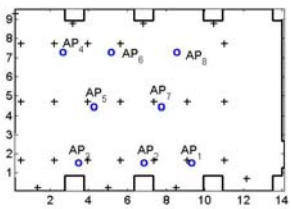

Figure 1. Sketch of the experimental geometry conference room (EUT1): APs (o) and calibration points (+). Dimensions are meters.

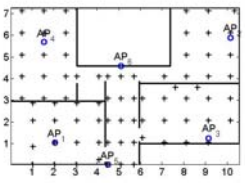

Figure 2. Sketch of the experimental geometry laboratory (EUT2): APs (o) and calibration points (+). Dimensions are meters.

II. POSITIONING ALGORITHM

A. Modeling Background

The numerical modeling used to produce the perturbed maps is a 2D ray tracing solver. The geometry of the environment under test is filled with scatterers with given electromagnetic properties.

At each location (x_i,y_i) the power received from AP_k is computed as:

$$\hat{P}_{k,i} = \left| \sum_{h=1}^{N_R} \frac{1}{L_h} \left(\prod_{j=1}^{M} \rho_{h,j} \right) e^{j\omega\tau_h} e^{j\alpha_h} \right|^2 \qquad (1)$$

where $e^{j\alpha_h}$ is the phase contribution due to the interaction (reflection or transmission) and $e^{j\omega\tau_h}$ is the phase delay contribution at the frequency of operation ω for delay τ_h; L_h is the path length associated to the h-th ray. $\prod_{j=1}^{M} \rho_{h,j}$ accounts for the intensity reduction due to the j-th reflection and/or transmission (up to M) experienced by the h-th ray.

The quality of the predictions is quantified by the RMS error between the computed values, $\hat{P}_{k,j}$, as given by (1), and the measurements, $P_{k,j}$, collected during the validation campaigns performed in both environments:

$$RMSE_{AP_k} = \left[\frac{1}{N_R} \sum_{i=1}^{N_R} \left(P_{k,i} - \hat{P}_{k,i} \right)^2 \right]^{1/2} . \qquad (2)$$

The values $\hat{P}_{k,j}$ of the perturbed maps were adjusted with the measurements to match the average received power level. The values computed by the ray tracing have a dynamic range comprised between 0 and 1, while the actual values depend on the AP power level.

The overall RMS error, defined as:

$$RMSE = \frac{1}{N} \sum_{k=1}^{N} RMSE_{AP_k} \qquad (3)$$

is about 7 dB (EUT1) and 10 dB (EUT2).

B. Attenuation Maps Database

The perturbed attenuation maps are organized in two distinct databases.

Database1 (EUT1) is composed of 150 maps with 5 up to 10 scatterers, while database2 (EUT2) consists of 120 maps with 8 up to 60 scatterers. In both cases scatterers are modeled as polygons having at least 10 sides and their dimensions are set in terms of the radius r of the circumscribed circle (0.05 m≤r≤0.25 m). The spatial resolution is 0.1 x 0.1 m^2. Fig. 3 shows the database structure. Predicted attenuation values at the receiver location (x_i,y_i) are stored in columns, one for each AP.

The reference map used in the positioning algorithm is the average of the perturbed maps.

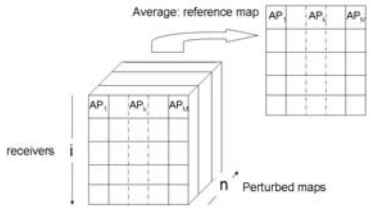

Figure 3. Structure of the attenuation maps database

C. Database representativeness

To assess the databases representativeness, in both environments a validation campaign was performed avoiding external sources of disturbances. For the receiver located at (4.4,2) Fig. 4a shows the measurements taken in EUT1 over 120 seconds with people moving around the room, while Fig. 4b shows the numerical predictions given by 120 maps randomly chosen from database1.

The relation between prediction and measurements indicates ergodicity. That is, exchanging time as independent variable of the measurements with the index of the maps shows equivalence of variability. Also, this example suggests that the number and/or the dimensions of the scatterers should be increased to obtain a better agreement as far as the dynamic range is concerned.

D. Localization

In both environments, the localization of the point under test (probe node) is implemented in such a way to mimic an actual application.

One perturbed map has been picked from the database and it is chosen as a snapshot of the received power map. The tuple $\{a_k(x_i,y_i)\}$ of the attenuation values read from the map is assigned at the probe location (x_i,y_i). Then, the optimization algorithm evaluates the cost function K defined as:

$$K(j) = \sqrt{\sum_{k=1}^{N_{AP}} \left(< a_k(x_j, y_j) > - a_k(x_i, y_i) \right)^2} \quad ,(4)$$

where $<a_k(x_i,y_i)>$ is the attenuation value read from the reference map at point (x_i,y_i) when AP_k is transmitting.

The outcome of the algorithm is $(x_j,y_j) \rightarrow K$ is minimum. The quality of the single retrieval is given by the distance error ε_i in the model space:

$$\varepsilon_i = \sqrt{(x_j - x_i)^2 + (y_j - y_i)^2} \; . \qquad (5)$$

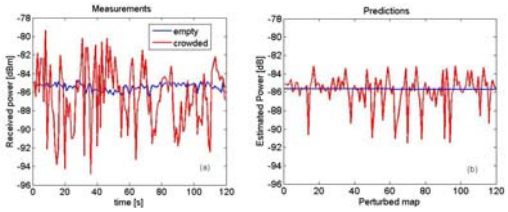

Figure 4. Comparison between measurements (a) and predictions (b) for the receiver located at (4.4,2) in EUT1

E. Tracking

Whichever the method for tracking, the basic idea is that the user motion does not happen randomly, but there is some correlation between the current and the previous positions. Among the different approaches, real-time tracking could be performed by using filtered values of the RSSI values [6, 7].

As the proposed technique works with simulated attenuation map values, the tracking algorithm is tailored to this specific case. For sake of simplicity, the author's main assumptions concern the computation of a *mean displacement vector*, the choice of an uncertainty range R and of an hysteresis interval of 4 points. As a consequence, the first 4 points are located as reported in §II.D. After this stage, the current displacement vector is computed as the difference between the actual and the previous estimated location:

$$\bar{d}_i = (\hat{x}_i - \hat{x}_{i-1})\bar{1}_x + (\hat{y}_i - \hat{y}_{i-1})\bar{1}_y \qquad (6)$$

To increase the robustness of the technique, a training period is introduced. The mean displacement vector, is computed as the sliding average of the previous 4 displacement vectors:

$$\left\langle \bar{d}_j \right\rangle = \frac{1}{N_P} \sum_{j-N_P}^{j} \alpha_i \bar{d}_i \,, \qquad (7)$$

where N_P is the number of the samples introduced in the training process (=4 in this case) and α_i is a coefficient that weights the single vector contribution in such a way that farther values count less than closer ones. Namely, the weighting coefficient is:

$$\alpha_i = \frac{(N_P{}^2 - N_P \cdot i)}{\sum_{i=0}^{N_P-1} (N_P{}^2 - N_P \cdot i)} \qquad (8)$$

The vector $\left\langle \bar{d}_j \right\rangle$, located in the previous estimated position, P_j, points to the next most probable location of the probe, P_p, as depicted by the big arrow in Fig. 5. The uncertainty range R is used to trace a circle that indicates the most probable area in which the position retrieval agrees with the motion history. The value of R is related to the dynamic range of the received power as predicted by the perturbed map for each database.

Hence, the actual position is retrieved through (4) and if it is within the circular region of Fig. 5, it is accepted and the algorithm updates the mean displacement vector and the starting point. It could happen that the static localization results in a point that falls outside the circular region due to numerical minima of (4) that give a wrong localization or due to sudden changes in the probe node motion. To protect the algorithm from false minima this point is discarded and P_p is taken as the actual position. If during the tracking process the static retrieval restitutes three times consecutively a point outside the circular area, it means that the motion has changed. A reset is performed and the tracking restarts from this point: the first 4 points are located statically, the mean displacement vector is computed with (6) and so on.

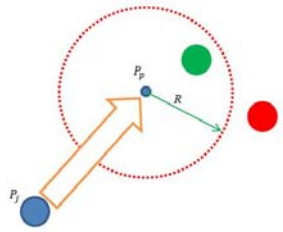

Figure 5. Sketch of the error detection/correction in the tracking algorithm by means of the mean displacement vector (big arrow) and the intrinsic uncertainty range (small arrow). P_j and P_p are the previous estimated and the next most probable points, respectively.

All the parameters, such as the length of the hysteresis interval, the values of uncertainty range R and of the weighting coefficients in (6), the number of refused localizations are the outcome of an heuristic approach and they are strongly dependent from the environment. Hence, a training test is mandatory when applying the algorithm for the first time.

III. NUMERICAL RESULTS

A. Localization

The overall performances of the proposed algorithm are evaluated by means of the bias, i.e. the mean value of the distance error, for the whole database:

$$< \varepsilon_i >= \sum_{j=1}^{N_M} \frac{\varepsilon_i}{N_M} \qquad (9)$$

where N_M is the map number in the database.

Figs. 6 and 7 show the bias value for EUT1 and EUT2, respectively. In Fig. 6 the localization acts satisfactory in the leftmost region of the conference room, showing a value lower than 0.5m in almost all position, while the rightmost one presents position with a bias error greater than 2m.

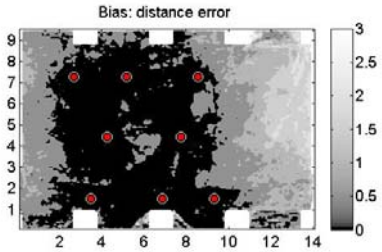

Figure 6. Map of the bias values for EUT1. Dimensions are meters. Circles represent the APs' actual position.

The reason for this twofold behavior is in the non homogeneous AP deployment: the localization of the position in the region without AP appears to be influenced by local fluctuations of weak power signals.

Again, in EUT2 the localization performs better in the best covered area, as in the lobby or close to the AP nodes.

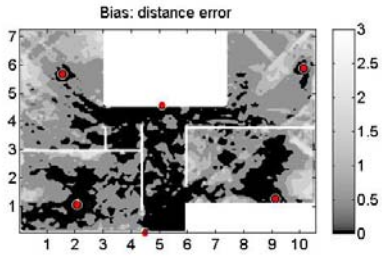

Figure 7. Map of the bias values for EUT2. Dimensions are meters. Circles represent the APs' actual position.

A quantitative evaluation of the performances is given by the cumulative distribution functions (CDFs) of the bias for both environments as depicted in Fig. 8.

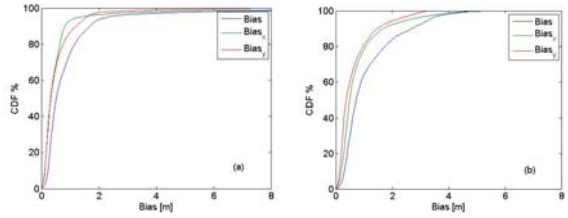

Figure 8. Cumulative distribution function of bias computed in EUT1 (a) and in EUT2 (b).

Table 1 reports the values of the bias and the RMSE of the distance error at three chosen probability levels. The RMSE is computed in order to evaluate the standard deviation of the bias. As expected, EUT1 shows better results in terms of bias, while the RMSE does not evidence specific trends.

TABLE I.
ERROR INDICATOR VALUES AS A FUNCTION OF THE CDF PROBABILITY LEVEL.

CDF	EUT1s		EUT2	
	Bias [m]	RMSE [m]	Bias [m]	RMSE [m]
10%	0.21	0.45	0.31	0.43
50%	0.47	0.91	0.71	1.02
90%	1.71	2.37	2.7	2.61

B. Tracking

At the time of writing, the author is still refining the tracking process for both environments.

The preliminary results of the tracking algorithm inside EUT1 are shown in Fig. 9. Fig. 9a shows the estimated path obtained through "static tracking", i.e. all positions are retrieved by using (4) without introducing any correlation or dynamic features, while Fig. 9b depicts the tracking result by using the algorithm described in II.E.

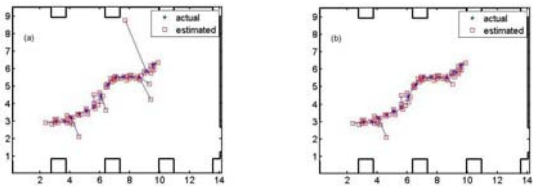

Figure 9. Tracking results: "static localization" along the path (a); tracking retrieval (b). Dimensions are meters.

One can notice the filtering of the outliers. At this stage, the chosen quantitative indicator is the RMS error relative to the path retrieval:

$$RMSE_p = \left[\frac{1}{N_{path}} \sum_{j=1}^{N_{path}} ((\hat{x}_i - x_i)^2 + (\hat{y}_i - y_i)^2) \right]^{1/2} \quad ,(10)$$

where N_{path} is the number of points along the path, (x_j,y_j) and $(\hat{x}_i,\hat{y}_j)$ are the given and the estimated position, respectively.

For the example in Fig. 9, $RMSE_p$ reduces from 0.65m to 0.5m, when introducing the tracking features.

IV. CONCLUSIONS

This paper presents the results of a positioning and tracking algorithm based on numerical simulations of the RSSI values predicted inside two indoor environments with different geometry and characteristics.

Localization is performed with a bias error of 0.47 m and 0.71 mm in the 50% of cases in EUT1 and EUT2 respectively.

Tracking evaluation is still on progress.

At the conference the author will detail the algorithm improvements and its performances.

REFERENCES

[1] K. W. Kolodziej and J. Hjelm, *Local Positioning Systems: LBS Applicationa and Services*, Boca Raton, FL, CRC Press, 2006, pp. 149-150.

[2] M.F Iskander. and Z. Yun, "Propagation Prediction Models for Wireless Communications Systems", *IEEE Trans. on MTT*, Vol.50, No.3, pp 662-673, March 2002.

[3] A.V. Bosisio, "RSSI-based Localization and Tracking Algorithm for Indoors Environments," in *Proc. of Int. Conference on Electromagnetics in Advanced Applications ICEAA09,* pp. 469-472, Torino (I), Sept. 2009.

[4] C. Alippi and G. Vanini, "Wireless sensor networks and radio localization: a metrological analysis of the MICA2 received signal strength indicator", *Proc. of the First IEEE Workshop on Embedded Networked Sensors*, Tampa (FL,USA), Nov. 2004

[5] C. Alippi, A. Mottarella and G. Vanini, "A RF map-based Localization Algorithm for Indoor Environments", *Proc. of the IEEE International Symposium of Circuits and Systems ISCAS'05*, pp. 652-655, Kobe (Japan), May. 2005.

[6] Erin-Ee-Lin Lau and W-Y. Chung, "Enhanced RSSI-based Real-time User Location Tracking System for Indoor and Outdoor Environment", *Proc. of Int. Conf. on Convergence Information Technology ICCIT 2007*, pp. 1213-1218, Gyeongju (Korea), Nov 2007.

[7] C: Morelli, M. Nicoli, V. Rampa, U. Spagnolini, C. Alippi, "Particle Filters for RSS-based Localization in Wireless Snsor Networks: an Experimental Study", in *Proc. of Int. Conf. of Acoustics, Speech, and Signal Processing, ICASSP 2006*, pp. 957960, Toulouse (F), May 2006